Electronic Supplementary Information

Facile synthesis of 3D Pd-P nanoparticle networks with enhanced electrocatalytic performance towards formic acid electrooxidation

Jingfang Zhang, You Xu and Bin Zhang*
Department of Chemistry, School of Science, Tianjin University, and Collaborative Innovation Center of Chemical Science and Engineering (Tianjin), Tianjin 300072, China. E-mail: bzhang@tju.edu.cn

Experimental Details

1. Material Synthesis.

1.1 Chemicals: All chemicals are analytical grade and used as received without further purification.

1.2 Synthesis of Pd-P nanoparticle networks (NNs): In a typical synthesis of the Pd-P NNs, 0.01 g NaH_2PO_2 and 0.29 g Brij 58 were dissolved in 8 mL of water. 0.1 mL HCHO and 4 mL Na_2PdCl_4 (20 mM) were added to the solution with stirring, and the pH of the solution was adjusted to 10 by adding appropriate amount of NaOH. Next, the mixed solution was transferred into a Teflon-lined stainless-steel autoclave and kept at 150 ^oC for 8 h. Then it was cooled down naturally. The resulting product was washed by distilled water and absolute ethanol for several times, respectively, and dried in a vacuum oven at 40 ^oC for 6 h. The Pd NNs have also been prepared by the same route without adding NaH_2PO_2 into solution.

The Pd-P nanoparticles aggregates (NAs) were prepared under the similar conditions expect for Brij 58 replaced by sodium dodecyl sulfate (SDS) with the same molar quantity.

2. Electrochemical Measurements: Electrochemical measurements were carried out in a typical three-electrode cell consisting of a working electrode, a Pt wire counter electrode, and a saturated calomel reference electrode (SCE) performed using an electrochemical workstation (CHI 660D, CH Instruments, Austin, TX). A glassy carbon electrode (diameter d = 3 mm) decorated with catalyst samples were used as the working electrode. All potentials, if not specified, were recorded according to SCE in this work. For a typical procedure for fabricating the working electrode, 1 mg of Pd-P NNs catalyst was dispersed in 1 mL of a mixture solvent (the volume ratio of H_2O: ethanol: 5% Nafion is 4:1:0.025), and the mixture was sonicated for 20 min to get a homogeneous ink. Then 4 μL of the ink (containing 4 μg of catalyst) was dropped onto the working electrode and dried in flowing argon. The preparing processes for Pd NNs and commercial Pd/C (10 wt%, Johnson Matthey) working electrodes were similar to that of Pd-P electrode. The corresponding Pd loading for Pd NNs and Pd/C were the same to that of Pd-P NNs.

Specifically, cyclic voltammetrys (CVs) were performed in 0.5 M N_2-purged H_2SO_4 solution at a scan rate of 50 mV s^{-1}. The electrochemically active surface area (ECSA) of the catalysts can be calculated from the electric charges of reduction of monolayer Pd oxide with an assumption of 424 μC cm^{-2} according to the CV curves.[1]

For formic acid oxidation, CVs were performed in 0.5 M HCOOH + 0.5 M H_2SO_4 at a scan rate of 50 mV s^{-1}.

Chronoamperometry was tested in 0.5 M HCOOH + 0.5 M H_2SO_4 at 0.1 V (vs. SCE).

For CO stripping, high-purity CO was bubbled into 0.5 M H_2SO_4 for 30 min while keeping the electrode potential at 0 V vs. SCE. Dissolved CO was then purged out of the electrolyte by bubbling N_2 for 30 min. Two consecutive CVs were recorded for the catalysts between -0.2 and 1.0 V at 50 mV s^{-1}.

For electrochemical impedance spectra (EIS): The EIS were recorded at the frequency range from 100 kHz to 1 Hz with the three-electrode system.

3. Characterization: The scanning electron microscopy (SEM) images and energy-dispersive X-ray spectroscopic (EDX) analysis were taken with a Hitachi S-4800 scanning electron microscope (SEM) equipped with the Thermo Scientific energy-dispersion X-ray fluorescence analyzer. Transmission electron microscopy (TEM), high-resolution transmission electron microscopy (HRTEM) images and EDX elemental distribution images were obtained with FEI Tecnai G2 F20 system equipped with GIF 863 Tridiem (Gatan). Specimens for TEM and HRTEM measurements were prepared via dropcasting a droplet of ethanol suspension onto a copper grid, coated with a thin layer of amorphous carbon film, and allowed to dry in air. The X-ray diffraction (XRD) patterns of the products were recorded with Bruker D8 Focus Diffraction System using a Cu Kα source (λ= 0.154178 nm). X-ray photoelectron spectroscopy (XPS) analysis was performed on a PHII600 spectrometer (PE Co., U.K.) using Mg Kα / Al Kα radiation.

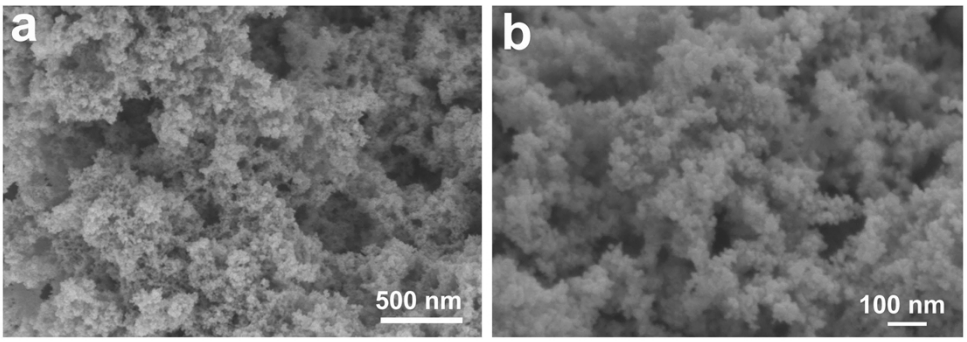

Fig. S1 (a, b) Representative SEM images of Pd NNs.

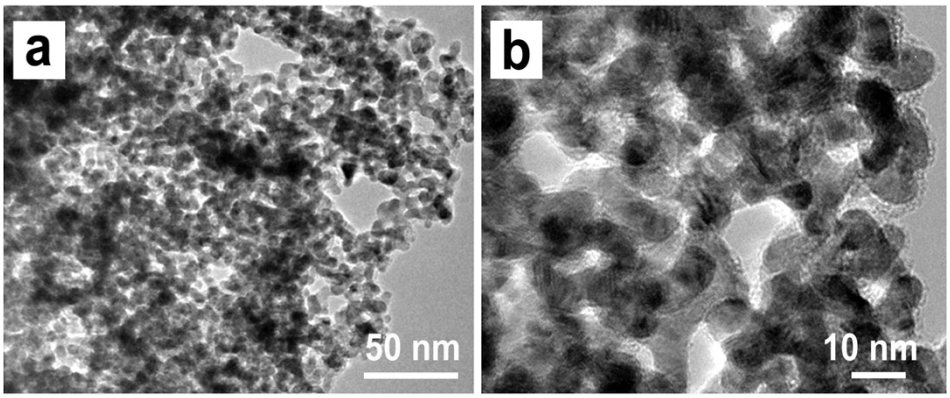

Fig. S2 (a, b) low-magnification TEM image (a) and high-magnification TEM image (b) of Pd NNs. The diameters of nanoparticles in the Pd NNs range from 5 nm to 15 nm.

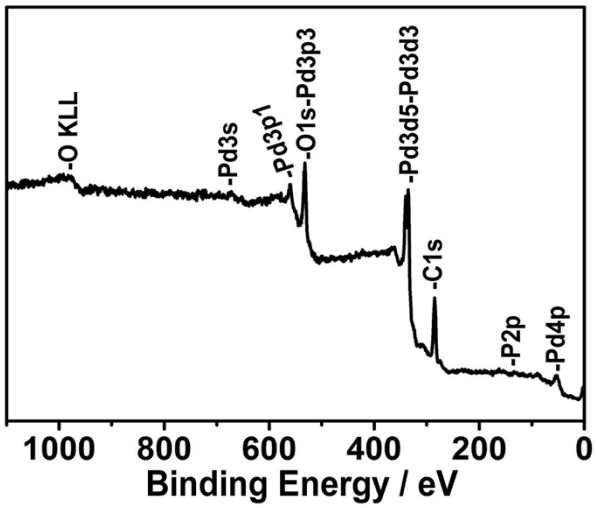

Fig. S3 XPS survey spectrum of Pd-P NNs.

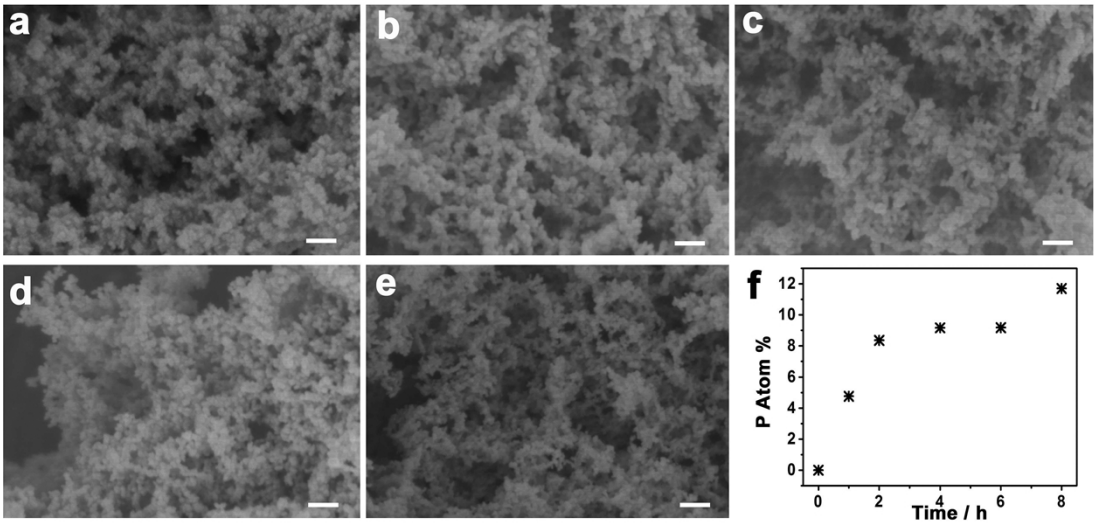

Fig. S4 (a-e) SEM images of the growth intermediates of Pd-P NNs produced after (a) 1 h, (b) 2 h, (c) 4 h, (d) 6 h, and (e) 8 h. The scale bars in these figures are 100 nm. (f) The dependence of the atomic ratio of P on the reaction time. The atomic ratios are calculated from the EDX spectra (they aren't provided here).

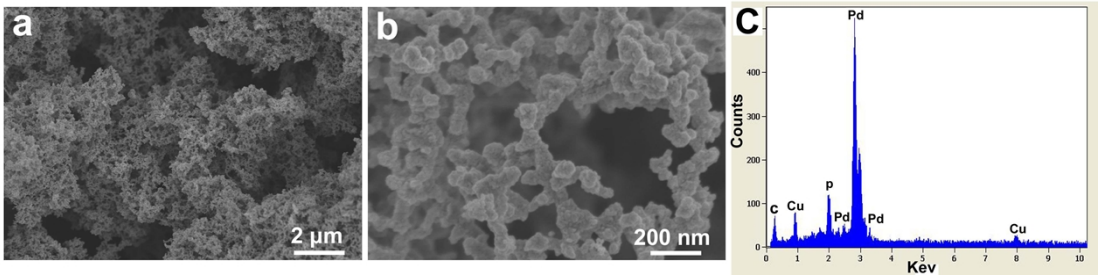

Fig. S5 (a, b) SEM images of Pd-P samples (named PdP-2 NNs here) prepared under the similar conditions in the synthesis of Pd-P NNs but excessive amount of NaH_2PO_2 (0.03 g) was used. (c) EDX spectrum of PdP-2 NNs. The detected Cu singles arise from the Cu foil on which the samples were deposited.

The PdP-2 NNs with much larger diameter (~ 100 nm) of nanoparticles were observed. The as-prepared PdP-2 NNs are composed of Pd and P with the atomic ratio of 4.1:1 (Pd to P).

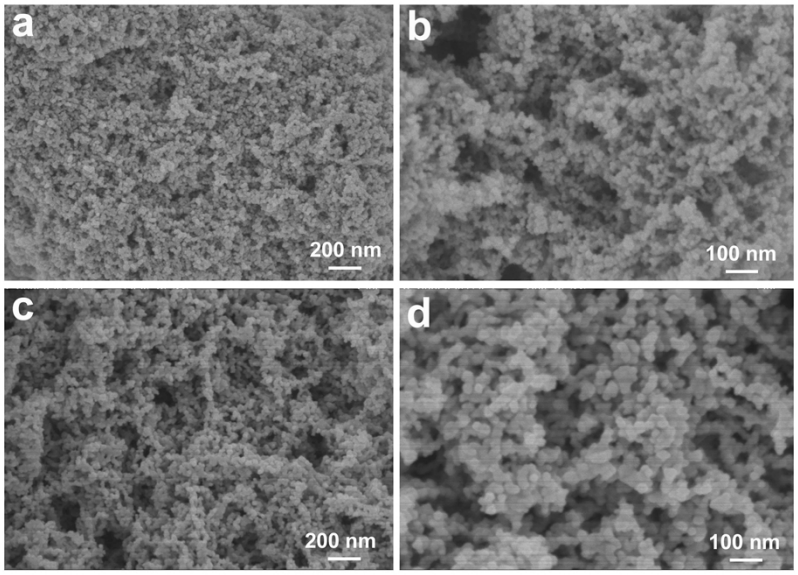

Fig. S6 (a-d) SEM images of Pd-P samples produced under different reaction conditions: (a, b) 120 ^{o}C and (c, d) 180 ^{o}C. Other synthesis conditions were similar to that of the typical synthesis. Decreasing the reaction temperature from 150 ^{o}C to 120 ^{o}C cannot led to satisfactory Pd-P NNs. Increasing the reaction temperature to 180 ^{o}C produced Pd-P NNs with much larger diameter of nanoparticles.

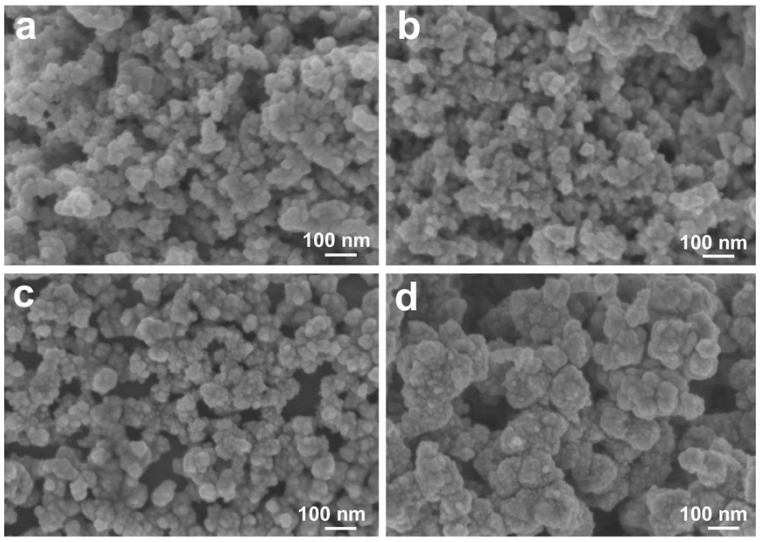

Fig. S7 (a-d) Representative SEM images of the products collected from reactions with similar conditions used in the synthesis of Pd-P NNs but (a) in the absence of Brij 58, (b) changing Brij 58 into hexadecyltrimethylammonium chloride (CTAC), (c) changing Brij 58 into poly(vinyl pyrrolidone) (PVP) and (d) changing Brij 58 into sodium dodecyl sulfate (SDS). All of the products synthesized with no surfactant (Fig. S5a) and other surfactants (CTAC, PVP, SDS; Fig. S5b-d) are completely different from those synthesized with Brij 58. Therefore, the presence of Brij 58 is critical for the formation of Pd-P NNs.

Based on the above-mentioned results, we propose a specious formation mechanism for the

NNs. The concentration of Brij 58 (C_{16}-EO_{20}; EO = ethylene oxide) used in this study is over critical micelle concentration (CMC), leading to the formation of spherical micelles coordinated with aqua-metal complexes. Since the water molecules interact with EO region of the micelles, the Pd ion species are entangled with the EO chains. Upon reduction, the Pd nuclei produces and grows gradually. Meanwhile, the element P generated by NaH_2PO_2 as shown in Eq. (1) can react with Pd nuclei to form Pd-P alloy nanoparticle.[2] Moreover, the Pd nanoparticles also act as catalyst to help P electroless deposition during reactions. While both water and EO regions are extruded with the grain growing, the EO chains involving the grown nanoparticle got distorted.[3] These as-formed distorted Pd-P nanoparticles further grow into network-like structure through particle fusion and Ostwald ripening. Finally, kinetic stable 3D networks composed of nanoparticles form through an Ostwald ripening mechanism.

$$3H_2PO_2^- \rightarrow H_2PO_3^- + H_2O + 2OH^- + 2P \quad (1)$$

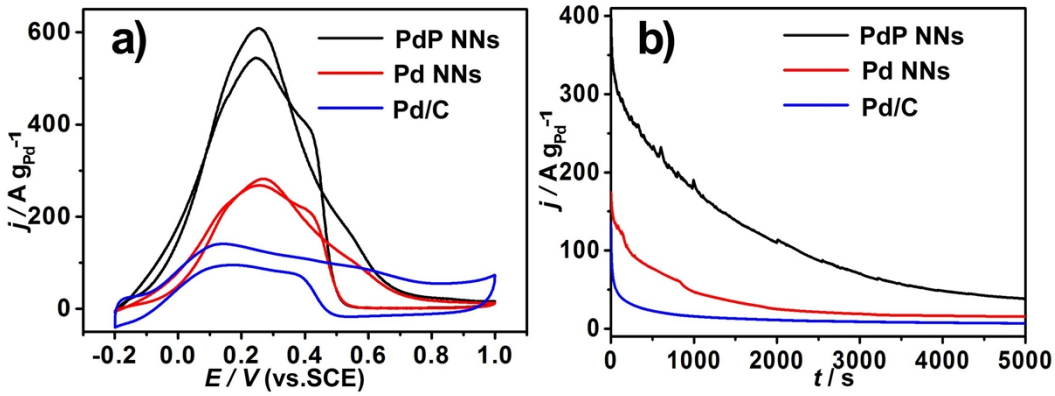

Fig. S8 Mass activity : CVs (a) and Chronoamperometry curves (b) of Pd-P NNs, Pd NNs and Pd/C catalysts in 0.5 M HCOOH + 0.5 M H_2SO_4 at a scan rate of 50 mV s^{-1}.

Table S1 Specific activity and mass activity of three catalysts at peak potential in 0.5 M HCOOH + 0.5 M H_2SO_4.

Catalysts	Specific Activity (mA cm^{-2})	Mass activity (A g_{Pd}^{-1})
Pd-P NNs	3.22	611.15
Pd NNs	2.32	285.66
Pd/C	0.89	142.71

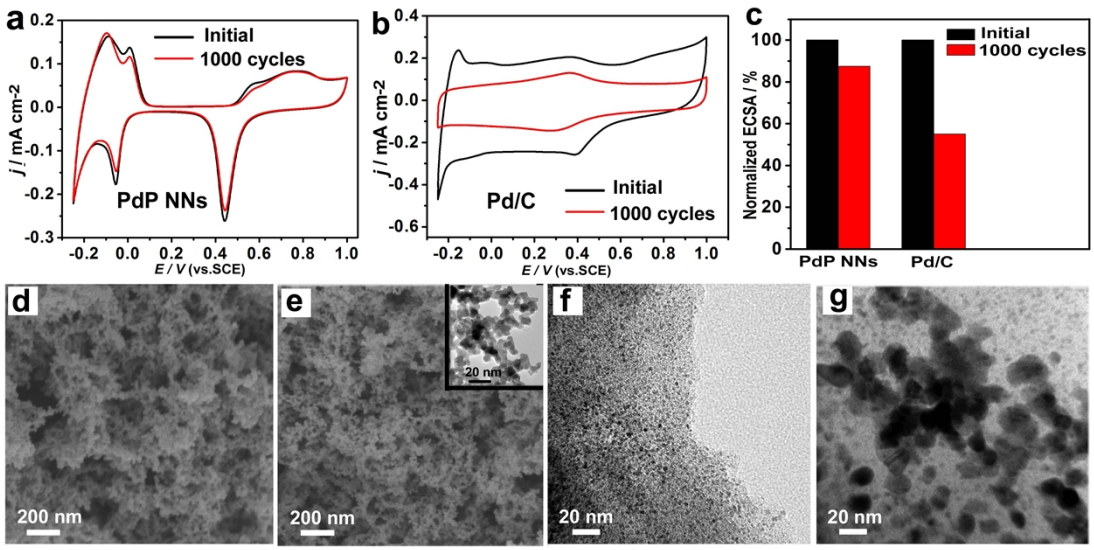

Fig. S9 (a, b) CV curves for Pd-P NNs (a) and Pd/C (b) catalysts after prolonged cycles of CV in 0.5 M N_2-purged H_2SO_4 at a scan rate of 50 mV s^{-1}. (c) Loss of ECSAs of Pd-P NNs and Pd/C catalysts after potential sweep cycles. (d, e) Representative SEM images of Pd-P NNs before (d) and after (e) 1000 cycles at a scan rate of 50 mV s^{-1}. The inset of (e) is the TEM image of Pd-P NNs sample collected after potential sweep cycles. (f, g) TEM image of commercial Pd/C catalyst before (f) and after (g) 1000 cycles at a scan rate of 50 mV s^{-1}.

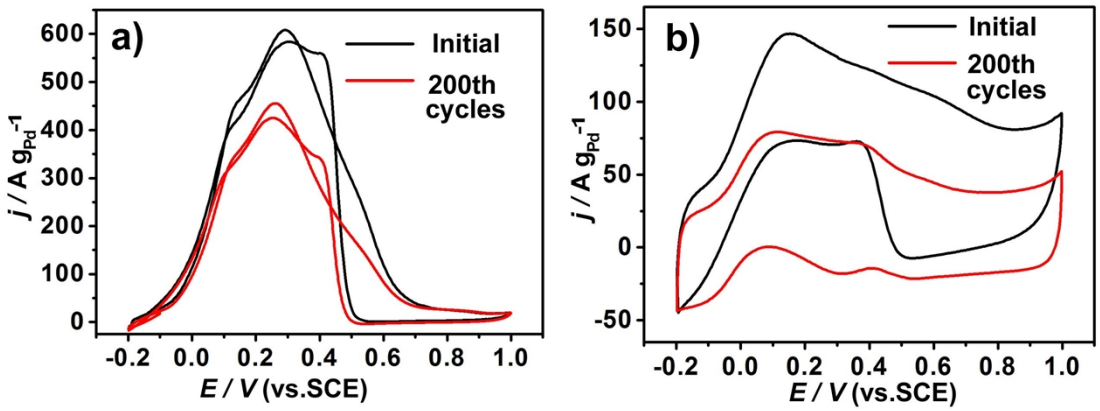

Fig. S10 (a, b) CV curves for Pd-P NNs (a) and Pd/C (b) catalysts after prolonged cycles of CV in 0.5 M HCOOH + 0.5 M H_2SO_4 at a scan rate of 50 mV s^{-1}. Pd-P NNs and commercial Pd/C showed losses of 25% and 43% in mass activity after 200 cycles, respectively.

From Fig. S9 and Fig. S10, one can see that Pd-P NNs exhibit better electrochemical durability than commercial Pd/C. It can be attributed to stable net-like framework which can effectively suppress the aggregation and sintering, leading to the maintenance of a larger number of active facets and the higher ECSA.

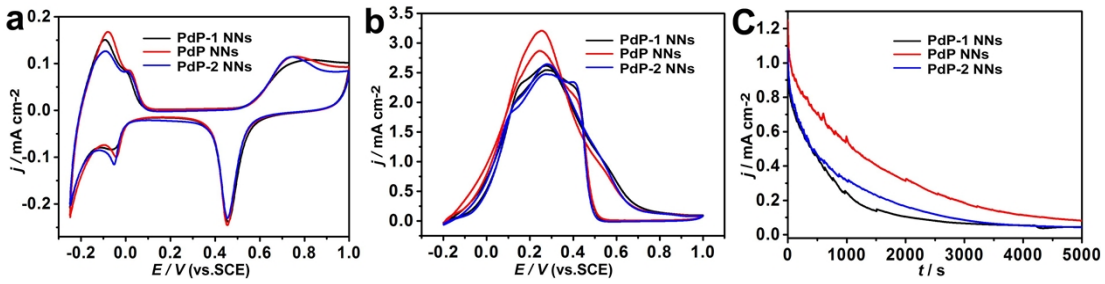

Fig. S11 Measurements of three Pd-P samples with different atomic ratios of Pd to P : PdP-1 NNs (20.0:1), Pd-P NNs (7.5:1) and PdP-2 NNs (4.1:1). (a) CVs of three Pd-P samples in 0.5 M N_2-purged H_2SO_4 at a scan rate of 50 mV s^{-1}. (b, c) CVs (b) and Chronoamperometry curves (c) of three Pd-P samples in 0.5 M HCOOH + 0.5 M H_2SO_4 at a scan rate of 50 mV s^{-1}. The PdP-1 NNs was collected from 1 h during the preparation of Pd-P NNs (Fig. S4a). The PdP-2 NNs was synthetized by adding 0.03 g NaH_2PO_2 with other conditions unchanged (Fig. S5).

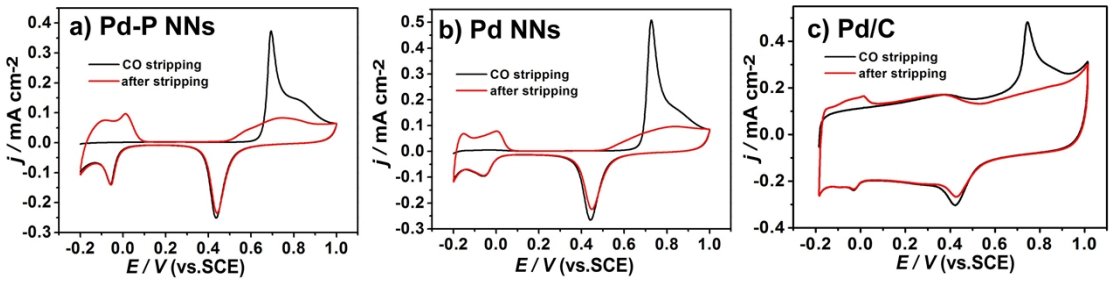

Fig. S12 CO stripping measurements of Pd-P NNs (a), Pd NNs (b), and Pd/C (c) catalysts in 0.5 M H_2SO_4 at 50 mV s^{-1}. The disappearance of CO stripping peaks after stripping and reappearance of hydrogen peaks at negative potentials indicate that all the catalysts are free of dissolved CO.

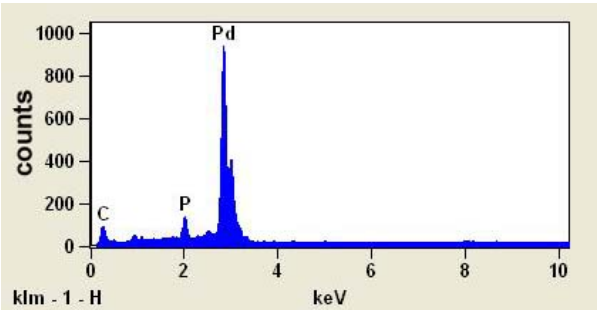

Fig. S13 EDX spectrum of Pd-P NAs. The atomic ratio of Pd to P is similar to that of Pd-P NNs.

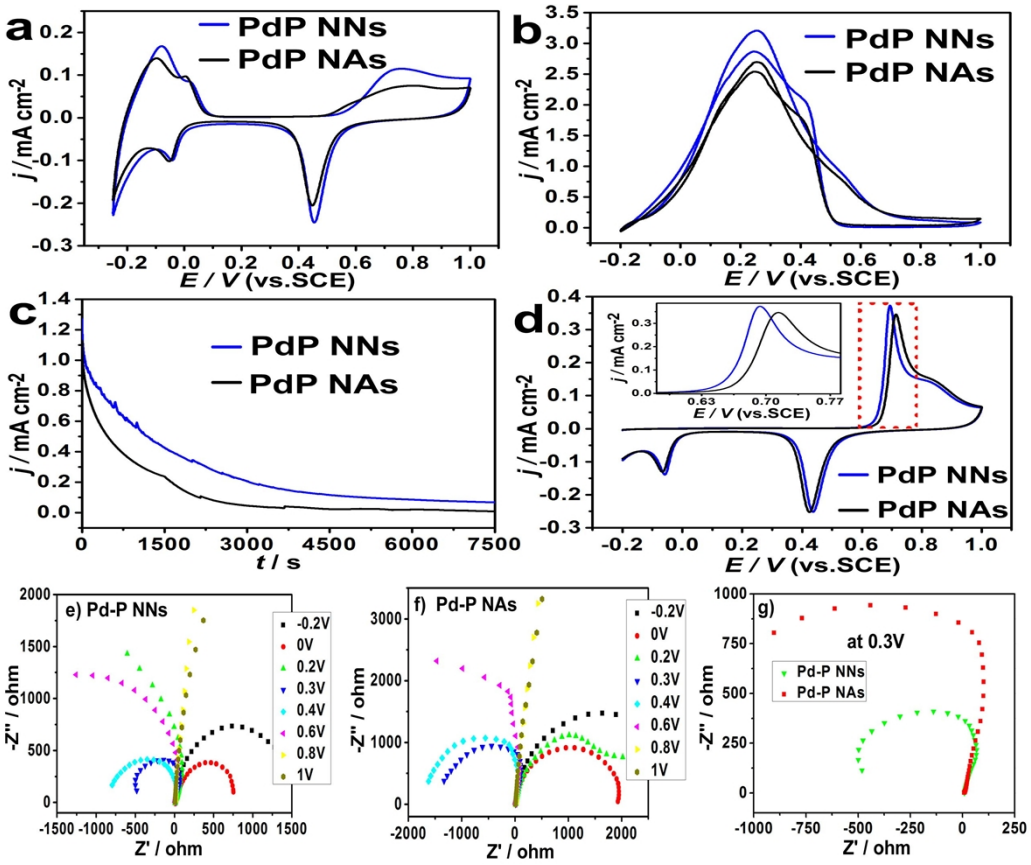

Fig. S14 (a) CVs of Pd-P NNs and Pd-P NAs in 0.5 M N_2-purged H_2SO_4 at 50 mV s^{-1}. (b, c) CVs (b) and Chronoamperometry curves (c) of Pd-P NNs and Pd-P NAs in 0.5 M HCOOH + 0.5 M H_2SO_4 at 50 mV s^{-1}. (d) CO stripping measurements of Pd-P NNs and Pd-P NAs in 0.5 M H_2SO_4 at 50 mV s^{-1} in the first forward scan. Inserts: magnified area enclosed with red squares. (e-g) Electrochemical impedance spectroscopy of (e) Pd-P NNs, (f) Pd-P NAs at different potentials, and (g) for the different catalysts at 0.3 V in 0.5 M HCOOH + 0.5 M H_2SO_4.

The electrochemically active surface areas (ECSAs) are calculated to be 18.92 and 3.30 m^2 g_{Pd}^{-1} for Pd-P NNs and Pd-P NAs, respectively (Fig. S8a). Fig. S8b shows that the forward peak current density for FAER on Pd-P NNs is 3.22 mA cm^{-2}, which is about 1.19 times than that of Pd-P NAs (2.71 mA cm^{-2}). It is obvious that the Pd-P NNs exhibit a slower current decay and much higher current densities over time than Pd-P NAs (Fig. S8c). In Fig. S8d, we can see that the peak potential (0.69 V) of CO oxidation on the Pd-P NNs is obviously more negative than that of the Pd-P NAs (0.71 V). From Fig. S8e-g, it is found that formic acid can be easily oxidized at 0.3 V due to the reduced Pd active sites passivation.[4] Moreover, the Pd-P NAs have much larger reactive resistance than Pd-P NNs at 0.3V, indicating the lower activity of Pd-P NAs.

References

[1] D. A. J. Rand and R. Woods, *J. Electroanal. Chem.*, 1971, **31**, 29.

[2] K. Wu, X. Mao, Y. Liang, Y. Chen, Y. Tang, Y. Zhou, J. Lin, C. Ma and T. Lu, *J. Power Sources*, 2012, **219**, 258.

[3] H. Wang, L. Wang, T. Sato, Y. Sakamoto, S. Tominaka, K. Miyasaka, N. Miyamoto, Y.

Nemoto, O. Terasaki and Y. Yamauchi, *Chem. Mater.*, 2012, **24**, 1591.
[4] J. Chang, L. Feng, C. Liu, W. Xing and X. Hu, *Angew. Chem. Int. Ed.*, 2014, **53**, 122.